www.MaterialsViews.com

ADVANCED
FUNCTIONAL
MATERIALS
www.afm-journal.de

FULL PAPER

Single-Step Deposition of Au- and Pt-Nanoparticle-Functionalized Tungsten Oxide Nanoneedles Synthesized Via Aerosol-Assisted CVD, and Used for Fabrication of Selective Gas Microsensor Arrays

Stella Vallejos, Polona Umek, Toni Stoycheva, Fatima Annanouch, Eduard Llobet, Xavier Correig, Patrizia De Marco, Carla Bittencourt, and Chris Blackman*

Tungsten oxide nanostructures functionalized with gold or platinum NPs are synthesized and integrated, using a single-step method via aerosol-assisted chemical vapour deposition, onto micro-electromechanical system (MEMS)-based gas-sensor platforms. This co-deposition method is demonstrated to be an effective route to incorporate metal nanoparticles (NP) or combinations of metal NPs into nanostructured materials, resulting in an attractive way of tuning functionality in metal oxides (MOX). The results show variations in electronic and sensing properties of tungsten oxide according to the metal NPs introduced, which are used to discriminate effectively analytes (C_2H_5OH, H_2, and CO) that are present in proton-exchange fuel cells. Improved sensing characteristics, in particular to H_2, are observed at 250 °C with Pt-functionalized tungsten oxide films, whereas non-functionalized tungsten oxide films show responses to low concentrations of CO at low temperatures. Differences in the sensing characteristics of these films are attributed to the different reactivities of metal NPs (Au and Pt), and to the degree of electronic interaction at the MOX/metal NP interface. The method presented in this work has advantages over other methods of integrating nanomaterials and devices, of having fewer processing steps, relatively low processing temperature, and no requirement for substrate pre-treatment.

1. Introduction

Functional properties in materials may be improved by tailoring morphological and structural features of the surface to the nanoscale,[1] with enhanced functionality reported in nanostructured materials (NSMs) such as nanoparticles (NPs), nanodots (NDs), nanoneedles (NNs), nanorods (NRs) and nanobelts (NBs) as a result of their increased surface-to-volume ratio and unique surface chemistry compared to their bulk counterparts.[2] Alternative methods of tailoring the functional properties of materials include the introduction of intentional impurities (dopants) into the matrix, or by producing "composites" of different individual elements or compounds with materials comprised of a bulk semiconductor with metal NPs having demonstrated improved electronic and catalytic properties as a function of the individual metal NP characteristics (e.g., oxidation states, size, shape and distribution).[3] For instance, in metal oxide-based gas sensors, enhanced performance is typically achieved by decreasing the particle (grain) size[4] and/or by adding noble metal NPs to the surface, which is known to improve not only sensitivity and stability but also selectivity (the three S', the most important features for the performance of a gas sensor). In nanoparticles the surface states formed during gas adsorption effectively extend through the entire particle giving a dramatic increase in gas sensitivity.[5] In materials functionalized with metal NPs the effect exerted by the metal NP on the

Dr. S. Vallejos, Dr. C. Blackman
Department of Chemistry
University College London
20 Gordon Street, London, WC1H 0AJ, UK
E-mail: c.blackman@ucl.ac.uk

Dr. S. Vallejos
Instituto de Microelectrónica de Barcelona
Consejo Superior de Investigaciones Científicas
Campus UAB, 08193 Bellaterra, Barcelona, Spain

Dr. P. Umek
Solid State Physics Department
Jožef Stefan Institute
39 Jamovacesta, 1000 Ljubljana, Slovenia

Dr. T. Stoycheva, F. Annanouch, Dr. E. Llobet,
Dr. X. Correig
Departament d'Enginyeria Electrònica
Universitat Rovira i Virgili
Països Catalans 26, 43007 Tarragona, Spain

Dr. P. De Marco, Dr. C. Bittencourt
Laboratory of Plasma-Surface Interaction Chemistry
University of Mons
1 Copernic, 7000 Mons, Belgium

metal oxide support, and as consequence the ideal NP characteristics, are a matter of much debate, with the effect of these additives, and hence sensitivity towards a given analyte, varying according to the metal NP characteristics leading to modulation of the selectivity of the sensor. Several reports in the literature have corroborated this fact, pointing out the importance of using reduced metal-NP sizes <5 nm[6] and low concentrations of metal NPs,[7] which are thought to have a greater influence on the electronic structure of the support and in creating new adsorption sites.

The ability to combine methods of manipulating the properties of materials, (i.e., both synthesis at the nanoscale and functionalization), provides access to materials with potentially new and enhanced properties and various conceptual routes to functionalized NSMs are available,[8] based either on the synthesis and combination of the components separately (multistep) or by direct synthesis of the functionalized material (single-step). A variety of strategies towards such materials are described in the literature[8,9] although the use of single-step routes, despite potential fabrication advantages, is infrequently reported. The commercial exploitation of nanomaterials in real-world devices is a major driver in nanoscience and nanotechnology requiring synthesis techniques that are compatible with manufacturing processes, yet currently the synthesis of functionalized NSMs and their integration with device fabrication (i.e., for use in microelectronic devices) remains a research challenge. Chemical vapor deposition (CVD) is an industrially relevant technique that is scalable and can be integrated into device-manufacture strategies, however its use for synthesis of NSMs often requires the use of catalysts (e.g., vapor-liquid-solid approach)[2] and/or relatively high temperatures.[10] This means it has limited applicability for use with fragile or temperature sensitive substrates, for instance those based on micro-electromechanical systems (MEMS) fabrication.[11]

Recently we have demonstrated a new catalyst free, (relatively) low temperature single-step aerosol-assisted chemical vapor deposition (AACVD) method to thin films of tungsten oxide NNs functionalized with gold NPs,[12] achieved by tuning the degree of homogeneous and heterogeneous gas-phase reactions of both metal and metal oxide precursors. These NSMs were used as gas-sensing elements providing ceramic gas-sensor devices with high sensitivity.[12] Tungsten oxide was used due to its promising properties for gas-sensor applications,[13] with it having demonstrated high sensitivity to various gaseous species both in its intrinsic form, in particular NO_x[14] and O_3,[15] and when functionalized with noble metal NPs (e.g., Au, Pt and Pd), for instance to gases such as C_2H_6O,[12,16] H_2,[17] and H_2S.[18]

The high surface-to-volume ratio and large accessible surface of nanoscaled tungsten oxide synthesized via AACVD allows the use of very small amounts of this material as the active sensing layer compared to bulk material, in turn enabling microsensor (MEMS) platforms to be utilized for devices. Miniaturization of sensors offers faster response times and lower detection limits than traditional ceramic sensors and both reduces

material consumption in device manufacture and reduces power consumption in device operation, enabling sensors to be deployed on-site and making real-time detection possible.[19] A particular advantage of the AACVD technique that indicated it might be suitable for use in microsensors is the relatively low temperature of deposition compared to other CVD methods of NSM synthesis,[10] which is essential for compatibility with MEMS platforms.

In the present work, the AACVD technique has been further developed to provide a wider range of functionalized, nanostructured tungsten oxide-based materials and these have been deposited directly onto microsensors. This method has then been used to create a matrix of MEMS-based gas sensors with different sensing elements (i.e., non-functionalized and functionalized tungsten oxide with Au and/or Pt nanoparticles), where the unique characteristics of the individual nanomaterials have been exploited to differentiate and quantify analytes (EtOH, H_2, and CO) typically involved in proton-exchange fuel cells.[20]

2. Results

2.1. Film Analysis

AACVD using $W(OPh)_6$ or $W(OPh)_6$ co-reacted with $HAuCl_4 \cdot 3H_2O$ and/or $H_2PtCl_6 \cdot xH_2O$ resulted in the formation of adherent uniform films of tungsten oxide NNs, or tungsten oxide NNs functionalized with Au, Pt, or Pt/Au particles, on microsensor substrates. The films were characterized by a dark black color as-deposited, which after annealing became pale green for tungsten oxide (W) or gold-functionalized tungsten oxide (Au/W) films, and white for platinum (Pt/W)- or platinum/gold (Pt/Au/W)-functionalized tungsten oxide films. Annealed films were used in the sensor devices in this work; SEM imaging of these films (**Figure 1**) showed a high density of non-aligned NNs with uniform diameters, which appeared identical for both non-functionalized and functionalized films. Cross section of the films showed NNs with lengths of ≈7 µm and diameters ranging between 60 and 120 nm, corresponding to aspect ratios of ≈60–115. This is consistent with our previous work on deposition of W and
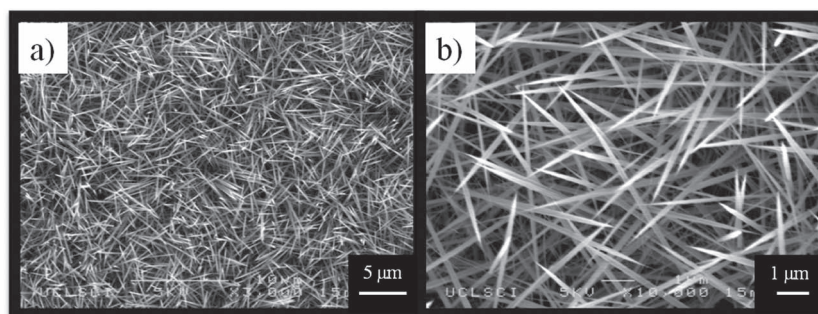

Figure 1. Film morphology observed by SEM images at low (a) and high (b) magnification. Non-functionalized (W) and functionalized NN films with gold (Au/W), platinum (Pt/W), and platinum/gold (PtAu/W) show the same morphology.
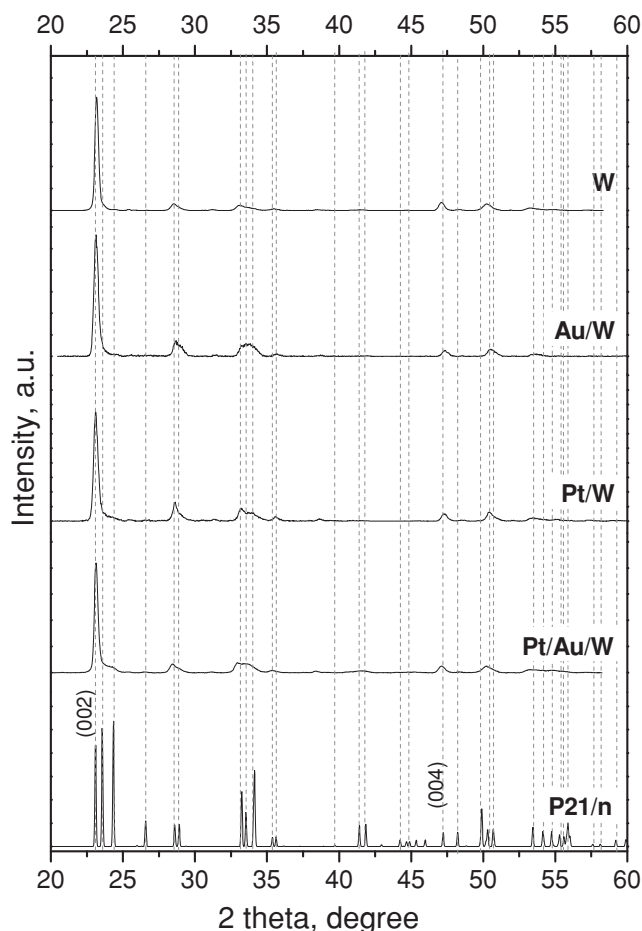
Figure 2. XRD patterns of the non-functionalized (W), and functionalized films with gold (Au/W), platinum (Pt/W), and gold/platinum (PtAu/W). All of the diffraction peaks in the data can be indexed to a monoclinic phase (P21/n), ICCD card no. 72-0677, with only peaks of greatly enhanced intensity (preferred orientation) specifically indexed.

Au/W films on ceramic or glass substrates.[12,14b,21] XRD analysis revealed the presence of monoclinic-phase WO_3 ($P2_1/n$ space group, a = 7.306 Å, b = 7.540 Å, c = 7.692 Å, and β = 90.88°; ICCD card no. 72–0677) in both non-functionalized and functionalized films (**Figure 2**) similar to our previous results for W and Au/W films deposited on ceramic or glass substrates.[12,21] The patterns indicate a strong preferred orientation in the [001] direction, showing intense diffraction peaks at 23.11° 2θ (d = 3.84 Å) and 47.23° 2θ (d = 1.92 Å), corresponding to the (002) and (004) reflections of this monoclinic phase. Gold and/or platinum diffraction peaks were not observed in functionalized films.

WDX analysis of annealed films showed they were oxygen deficient (anal. calcd. for WO_3: W 24.98, O 74.99 at%; found: W 27, O 69 at%; O/W ratio 2.6) and contained an average of 2.5 at% carbon. In addition, functionalized films showed 0.09 at% (0.3 wt%) gold in Au/W films, 0.22 at% (0.70 wt%) platinum in Pt/W films, and both 0.03 at% (0.10 wt%) gold and 0.08 at% (0.23 wt%) platinum in Pt/Au/W films, with an average of 0.02 at% chlorine. XPS analysis similarly indicated

O/W ratios of 2.4 for W and Au/W films, 2.8 for Pt/W films, and 2.6 for Pt/Au/W films, and the absence of chlorine at the surface of the functionalized sensing films. These results are in agreement with our recent XPS study of W and Au/W NN films.[22] Thermal decomposition studies of the metal precursors (i.e., $HAuCl_4$[23] and H_2PtCl_6)[24] suggest metallic gold and platinum are obtained at the deposition temperature used in this work, consistent with the negligible chlorine contents, measured by WDX and XPS in all of the functionalized films. A comparison of the metal:tungsten ratio present in the precursor solution used for AACVD (anal. calcd. for Au:W 9.8%, Pt:W 9.7%) and the one determined by WDX in the sensing films (found for Au:W 0.4%, Pt:W 1%) show the incorporation of metal NPs is only ≈5–10% efficient, although the system has not yet been optimized for this parameter, and that the yield for gold NP loading is half the yield of platinum NP loading. The sensing films comprising a mixture of both platinum and gold precursors (anal. calcd. for Au:W 4.9%, Pt:W 4.8%) show similar incorporation efficiencies (found for Au:W 0.1%, Pt:W 0.3%) to those found for each metal precursor alone. The low metal loadings are the likely explanation for the lack of observed diffraction peaks in the XRD data.

TEM (**Figure 3**) of an NN showed the presence of well-dispersed metal nanoparticles (Au, Pt or Au/Pt) along the surface of the NN, consistent with results seen previously for gold-NP-functionalized tungsten oxide NNs on ceramic substrates.[12] Overall, the particles displayed approximately spherical morphologies, with sizes between 4–11 nm, 1–4 nm, and 1–11 nm for Au, Pt, and Au/Pt respectively (histograms for a total population of 100 particles are displayed in Figure 3). High-resolution TEM images exhibit highly ordered crystalline NN structures with marked planar spacing of approximately 3.88 ± 0.20 Å in all of the samples (i.e., non-functionalized and functionalized), consistent with the unit cell (c = 7.692 Å) observed by XRD and with previous results.[12,14b] The metal NPs display planar spacings of 2.35 ± 0.20 Å in Au/W and 2.21 ± 0.17 Å in Pt/W, consistent with the internal lattice spacing of the (111) plane of face-centred-cubic (fcc) gold (d = 2.355 Å, ICCD card no. 04–0784) or fcc platinum (d = 2.265 Å, ICCD card no. 04–0802), respectively. Films functionalized with gold and platinum NPs show planar spacings of 2.30 ± 0.16 Å in particles smaller than 4 nm, and 2.40 ± 0.11 Å in particles bigger than 4 nm, suggesting the presence of both platinum and gold NPs in these films.

Estimation of the activation energy for electrical conduction based on conductivity measurements between 200 °C and 350 °C in air revealed similar apparent energies for W (0.23 eV) and Au/W (0.21 eV) films, which are in agreement with earlier results reported for non-functionalized tungsten oxide films.[25] In contrast, platinum- and platinum/gold-functionalized films possess lower activation energy for conduction (0.09 eV). A comparison of the valence-band spectra recorded near the Fermi level ($E_B = 0$) on the non-functionalized and functionalized films is shown in **Figure 4**. The spectra are associated with the W 5d in-gap states, filled due to the presence of oxygen vacancies.[22] Results show that the presence of metal NPs at the surface of tungsten oxide NNs leads to new electronic states above the valence-band maximum of the oxide band gap, increasing the density of electronic states near the Fermi energy level. These
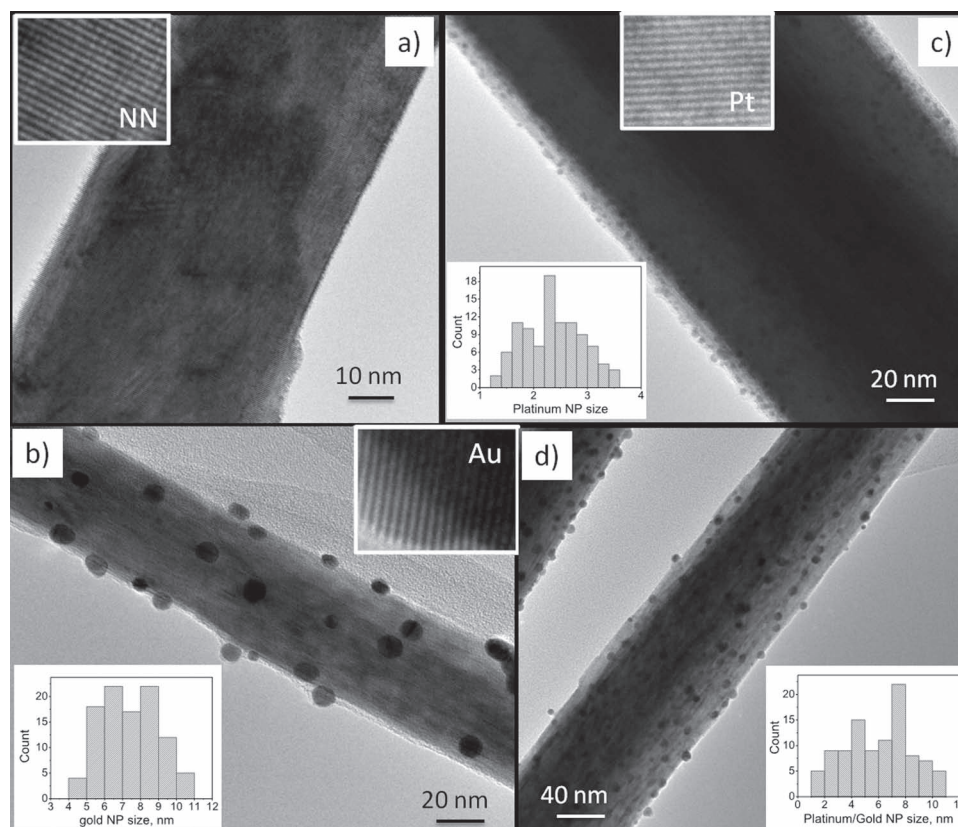
FULL PAPER

FULL PAPER

Figure 3. HR-TEM and size distribution of the non-functionalized (a) and functionalized samples with gold (b), platinum (c), and gold/platinum (d) NPs after annealing.

states are related to the "s-p" electronic band for Au/W films and 5d electronic valence-band for Pt/W films.[22,26]

2.2. Gas-Sensing Properties

Gas-sensing tests were carried out to ethanol, hydrogen and carbon monoxide by using dc resistance measurements. Non-functionalized and functionalized sensing films (W, Au/W, Pt/W, and Pt/Au/W) were tested at various sensor temperatures from 100–300 °C, in intervals of 50 °C, in order to determine the thermal dependence of the response to each analyte. General operating temperatures exceeding 200 °C showed little variation of the baseline resistance ($\pm 5\%$) over the whole testing period (see experimental details); at these temperatures the sensor response of both non-functionalized and functionalized films indicated good reproducibility with standard errors below $\pm 1\%$ and a tendency to reach a stationary state, or a saturated sensor response, after 300 s of analyte exposure, with complete recovery of the baseline resistance within 600 s after analyte removal. In contrast, operating temperatures less than 200 °C were characterized by drift of the baseline resistance, unsaturated sensor responses, and standard errors of up to $\pm 8\%$. Results (**Figure 5**) show that W films displayed maximum response to CO or H_2 at lower temperatures (150 °C) and to EtOH at higher temperatures (250 °C), whereas Pt/Au/W films

exhibit their greatest response to CO at 150 °C but to EtOH or H_2 at 250 °C. In contrast Pt/W and Au/W films showed their greatest response to CO, EtOH, or H_2 at the same temperature (250 °C). Figure 5 also shows the variation of the sensing response magnitude according to each type of film, revealing that platinum NPs considerably enhance the sensor response to H_2 (**Figure 6**) and modestly to CO at 250 °C, contrary to gold NPs which do not show response improvements to these analytes and to Pt/Au/W which displays only moderate improvement towards H_2. The reduced sensitivities observed for Pt/Au/W, relative to Pt/W, are likely a consequence of the lower content of platinum NPs in these films as determined by WDX (Pt/Au/W, Pt:W 0.3%; Pt/W, Pt:W 1%) and lack of available active sites on the tungsten oxide surface due to the presence of gold NPs. **Figure 7** displays the relative changes of the rate constant of functionalized films, compared to non-functionalized films, as a function of the temperature. The rate of response

Table 1. Power law constants for each sensor and analyte.

Analytes	Sensing film			
	W	Au/W	Pt/W	Pt/Au/W
CO	$0.37\ C^{0.25}$	$0.54\ C^{0.19}$	$0.51\ C^{0.30}$	$0.60\ C^{0.16}$
EtOH	$1.72\ C^{0.37}$	$1.34\ C^{0.32}$	$1.61\ C^{0.52}$	$1.23\ C^{0.25}$
H_2	$0.34\ C^{0.47}$	$1.43\ C^{0.16}$	$11.90\ C^{0.17}$	$1.65 C^{0.28}$

Materials
Views
www.MaterialsViews.com

ADVANCED
FUNCTIONAL
MATERIALS
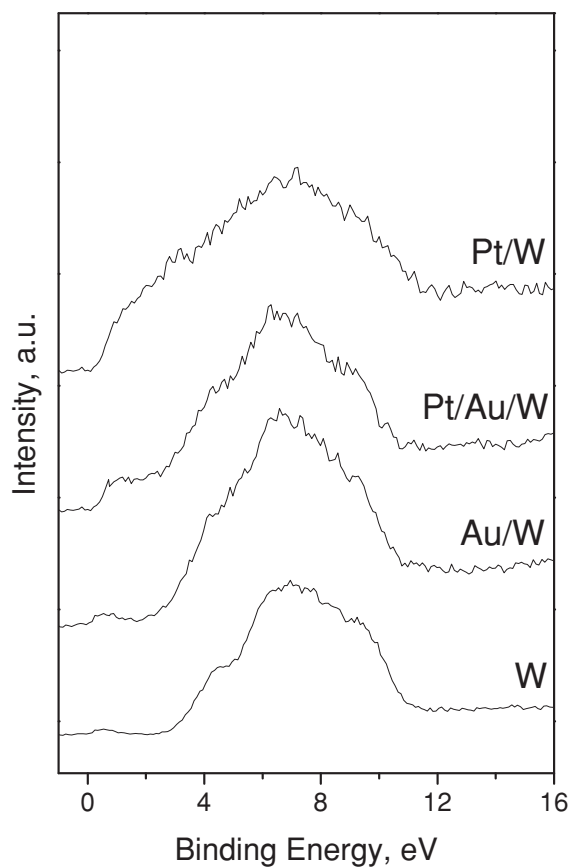www.afm-journal.de

FULL PAPER

Figure 4. Valence band from non-functionalized tungsten oxide NNs and functionalized tungsten oxide NNs with gold, platinum, and platinum/gold nanoparticles.
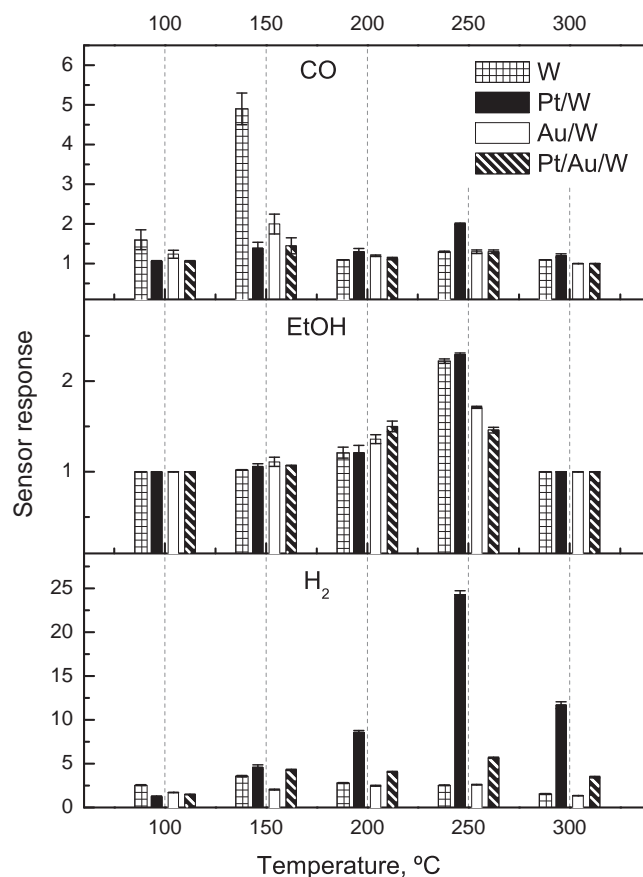

Figure 5. Sensor responses and error bars to 100 ppm of CO (a), 2 ppm of EtOH (b), and 100 ppm of H_2 (c) as a function of the operating temperature.

at each sensor operating temperature was estimated by fitting the change of resistance curve in the region from 2–8 minutes after target-gas (i.e., H_2, CO, and EtOH) injection to a logistic function, which was derived to obtain the rate law described by $-R/dt = rR^n$ (where r is the rate constant). The results presented in **Figure 8** show a direct dependence of the sensing response to the analyte concentration, with power-law fitting curves revealing different constants for each type of film (**Table 1** and inset in Figure 8). The prefactors (Table 1) indicate that sensitivity of tungsten oxide is enhanced to H_2 and CO by its functionalization with metal NPs, whereas results to EtOH show the opposite behavior.

Table 1 and Figure 5 indicate that Pt/W films have low cross sensitivities with H_2, suggesting good selectivity to this analyte, whereas the rest of films (W, Au/W, and Pt/Au/W) show some cross sensitivities to CO, EtOH, or H_2.
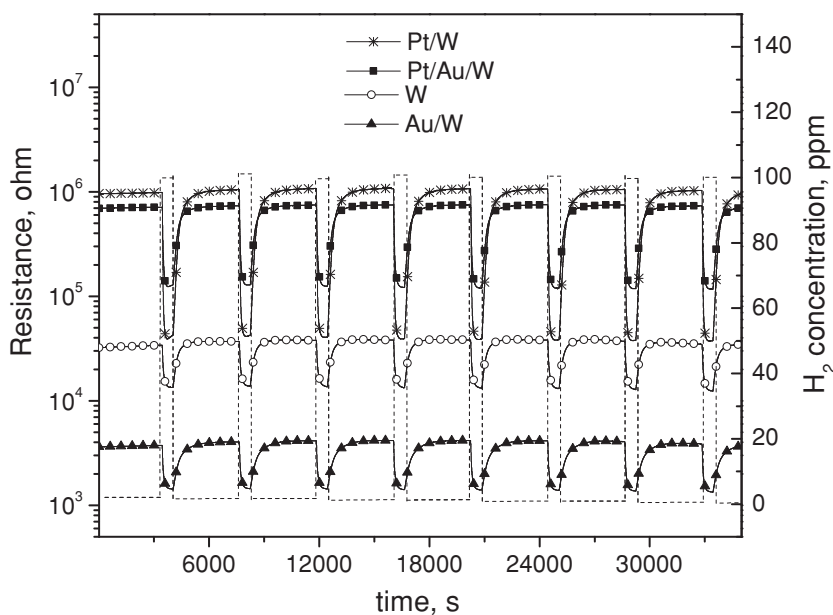

Figure 6. Film-resistance changes towards 100 ppm of hydrogen at 250 °C.
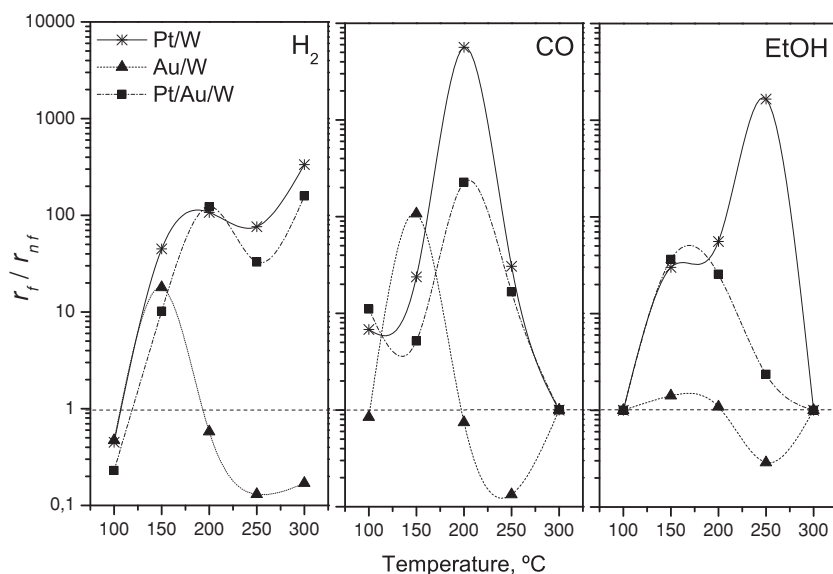
FULL PAPER

Figure 7. Relative change of the rate of response (r_f/r_{nf}) of functionalized (Au/W, Pt/W, Au/Pt/W) to non-functionalized (W) films as a function of sensor operating temperature.

3. Discussion

3.1. Film Analysis

Gold and platinum NPs synthesized via AACVD co-deposition method (Supporting Information, Section S1: film deposition) showed different size features (between 4–11 nm and 1–4 nm for Au and Pt respectively) with smaller particles observed for platinum NPs on tungsten oxide NNs, compared to gold NPs (Figure 2). An inverse relationship between the size of metal NPs after high temperature treatment and the melting point (MP) of the metal, as low as 600 K for small gold NPs, has been proposed,[27] with the larger size of gold NPs relative to platinum therefore consistent with the difference in bulk MP (Au 1336 K; Pt 2042 K) of the two metals. The reduced size of platinum NPs compared to gold NPs may also be explained by the presence of oxidation at the surface of the platinum NPs. Analysis of the Pt 4f core level spectrum recorded in the Pt-functionalized films (**Figure 9**), suggested the presence of Pt–O bonds, which is inferred from a low intensity doublet (2) shifted by 1.3 eV in the low binding energy respect to main doublet (1) ascribed to metallic platinum.[28] In contrast Au-functionalized films did not show the presence of Au–O bonds,[22] even though they may be present in very small Au clusters. Therefore platinum NPs may have enhanced interaction with the tungsten oxide surface compared to gold NPs due to the presence of an oxide shell, with the absence of Au oxidation providing higher mobility and hence increased particle size.[29] In addition it has been suggested that residual chloride could also cause increased particle size for NPs synthesized from chlorine containing precursors, particularly when using HAuCl$_4$, due to the high affinity of gold for chlorine. Initially the gold precursor has a Cl/Au molar ratio of 4 which diminishes to a notional molar ratio of 0.2 (assuming all of the Cl was bound to Au) after deposition, equivalent to 0.02 at% Cl detected by WDX in

the film. Although these values suggest relatively low chlorine contamination, previously it has been shown that a Cl/Au molar ratio of <0.01 may increase the probability of NP sintering,[30] hence this cannot be discounted. It is impossible to attribute the difference in gold and platinum NPs size to any one cause, however it should be noted that the NSMs deposited via this method show good stability once deposited with no changes observed in the structure, morphology or electrical resistance after gas-sensing measurements, conducted up to 300 °C.

3.2. Gas-Sensing Properties

Gas-sensing tests of functionalized and non-functionalized films registered good sensor responses to H$_2$, CO, and EtOH, which are comparable in magnitude or better than previous research.[14–18b,25,31] (Supporting Information, Section S2: comparative table). Surprisingly non-functionalized (W) films display a good response upon CO exposure (Figure 5) at low temperatures (<150 °C) and at low concentration (100 ppm), contrary to previous work in which tungsten oxide films, either polycrystalline on MEMS substrates[14a,18a] or nanostructured on ceramic substrates,[14b] were not sensitive to this analyte (Supporting Information, Section S3: CO sensing).

The small values of the exponent factors (less than 0.5), derived from the sensor response to different concentrations of the analytes (Table 1), suggest that NSM materials experience a complete depletion in flat band condition during analyte exposure.[32] As the exponent factors result from a combination of the adsorption or reaction of the analyte at the surface, and the changes of surface potential in the sensing film,[33] comparison of these values is problematic with no clear relation between the exponent factors and the sensitivity to each analyte. However, under these conditions it is likely that not only is the concentration of carriers taking part in conduction affected upon interaction with the analyte but also the carrier mobility can be affected, thus the relative change of electrical resistance (i.e., response magnitude) is influenced by both factors. Hall effect measurements were attempted on all of the sensing films but proved impossible due to the relatively high resistance of the various materials.

Principal component analysis (PCA)[34] was performed using up to ten replicates of the sensor responses (W, Au/W, Pt/W, and Au/Pt/W) to each sensed analyte at 250 °C, to evaluate the correlation between sensor response and selectivity of films. Sensor response data were mean-centered prior to performing PCA. **Figure 10** displays a visual appraisal of the discrimination of each analyte and its concentrations. The scores (i.e., the projections of measurements in a orthogonal base of PCs) in Figure 10a suggest that analytes (i.e., CO, EtOH, and H$_2$) and their corresponding concentrations could be discriminated by using an array of non-functionalized and functionalized sensing films, and as the maximum standard errors of the
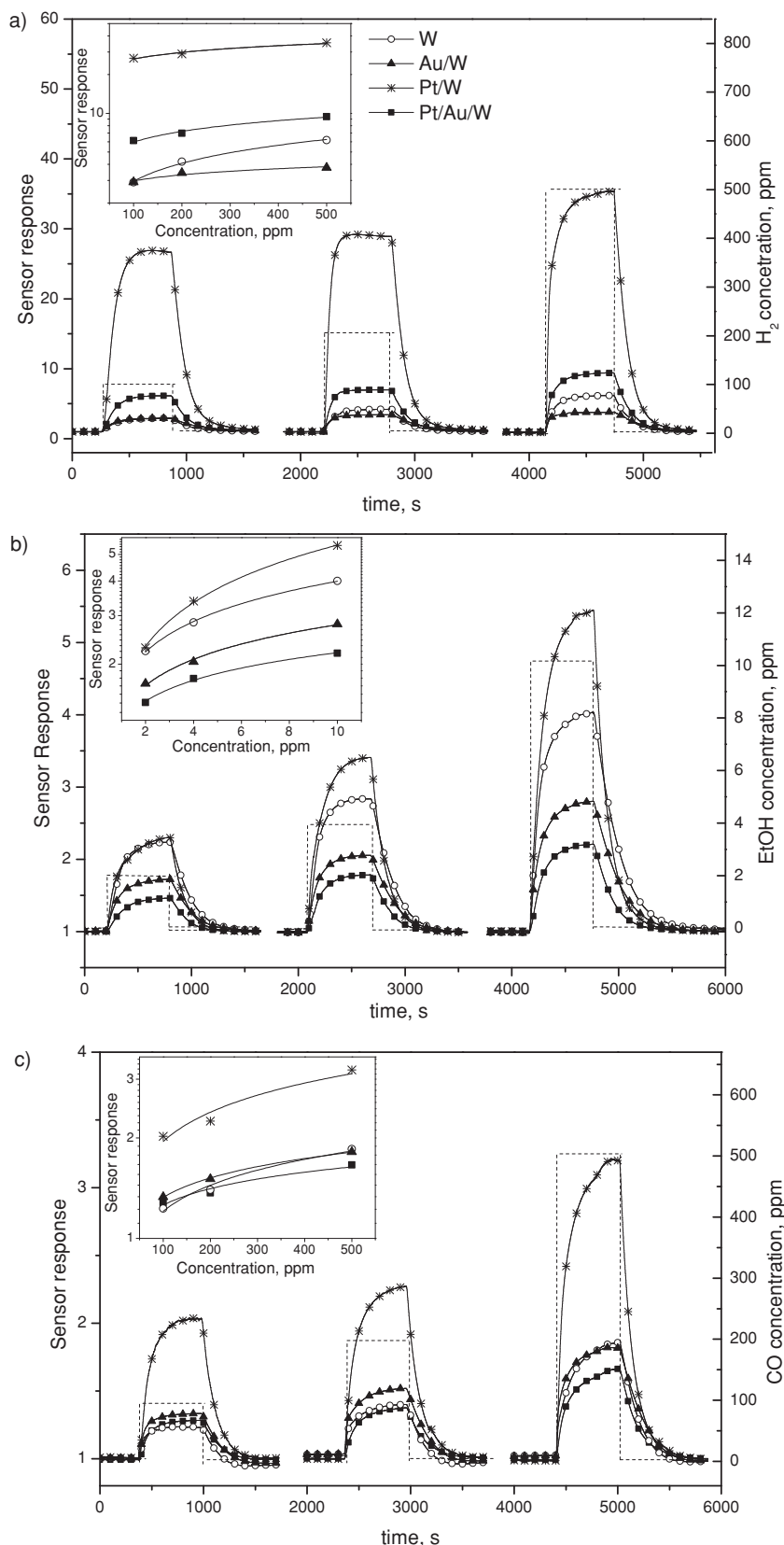
Figure 8. Sensor responses to various concentrations of H$_2$ (a), EtOH (b), and CO (c). The insets show the power-law curves of the response vs. concentration.

sensor response do not exceed ±1%, little dispersion of data is observed in each principal component. However, loadings (Figure 10b) indicate that Au/W and Pt/Au/W films contribute similarly to the discrimination, probably due to their similar sensing characteristics, and consequently the use of both sensing films in the array could be redundant. Conversely, Pt/W and W films are nearly uncorrelated since the former contributes mainly to principal component 1 and the latter to principal component 2. These results highlight the potential application of these structures in discriminating the analytes H$_2$, CO, and EtOH, which is a critical requirement in proton-exchange fuel cells.

3.3. Mechanisms of Gas Sensing

Currently, in the literature, two mechanisms are proposed to explain the role of metallic-like additives in gas sensing: spill-over (i.e., the enrichment of the MOX surface with reactive species through catalysis) and/or Fermi level control (i.e., changes in the chemical state of the metal NPs with active species).[3] Recent operando studies of gas sensing for metal NPs (Pd and Pt) supported on MOX have suggested a third mechanism, involving a local/surface site and an associate bulk effect due to the presence of oxidized, rather than metallic, states from the "metal" NPs, observable at low additive concentrations,[7] As both spill-over and Fermi level control have a similar effect on MOX (i.e., increasing or decreasing electrons in the conduction band), discrimination of their contribution is not straightforward from the current results. It is apparent that films with higher base line resistance (Supporting Information, Section S4: electrical properties) and lower activation energy of conduction (i.e., Pt/W and Au/Pt/W) gain in sensitivity, as these films showed enhanced sensor response and higher rate constants across the range of temperatures studied, contrary to Au/W films. It is possible that the oxidized states detected via XPS (Figure 9) in the "shell" surrounding the Pt particle and/or in the contact with the MOX during gas exposure contribute to Fermi level control at the NP/MOX interface, leading to the enhanced sensitivity observed for Pt/W.[29] In contrast Au functionalized films did not show the presence of Au–O bonds in XPS, even though their presence is suggested in very small Au clusters, which could be ascribed to the relatively larger size of gold NPs synthesized via co-deposition,
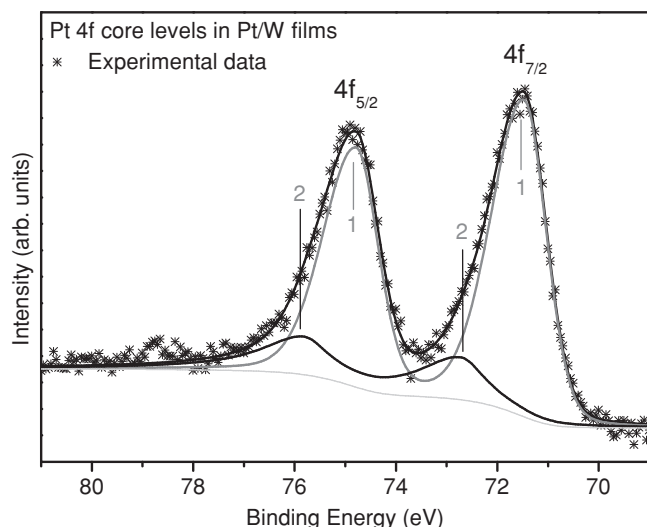
**ADVANCED
FUNCTIONAL
MATERIALS**

www.afm-journal.de

**Materials
Views**

www.MaterialsViews.com

Figure 9. Pt 4f core-level spectrum recorded on Pt-functionalized tungsten oxide films and its fitting curve. The doublet peak component "1" is generated by photoelectrons emitted from the Pt atoms forming metallic particles. The component "2" is associated with photoelectrons emitted from Pt atoms participating in Pt-O bonding. The background formed from secondary photoelectrons and is displayed in the light-grey color.

and hence little improvement in sensitivity is observed for Au/W films. Note however, we can not rule out the presence of Au–O species at the Au/NN interface. Previously it has been suggested that reduced sensor response time may be indicative of spill-over from the metal NPs to the support.[35] However the rate of response (Figure 7) show overall faster rates in Pt/W and Pt/Au/W films, whereas Au/W films show increased rates only at 150 °C and lower rates at all other temperatures. The abrupt decrease in rate of response above 150 °C in Au/W films to all of the analytes may be related to increased mobility of any residual chloride contamination selectively poisoning the active sites at the gold NP surface especially towards analytes forming hydroxyl groups when adsorbing at the MOX surface.[30] From our results we observe that an enhancement in the kinetics of response does not necessarily contribute to an improvement of sensor response. For instance, the increase in the rate of response for gold-NP-functionalized films to H$_2$ at 150 °C (Figure 5 and Figure 10), relative to non-functionalized films, may indicate that gold NPs act to catalyze H$_2$ detection on tungsten oxide NNs via spill-over (i.e., the gold NPs accelerate the dissociation of hydrogen molecules into H atoms), with sensing occurring from the formation of water molecules with the adsorbed oxygen and/or with the lattice oxygen of the tungsten oxide NNs,[17c] similar to the mechanism proposed for platinum.[17a] However, despite the increase in the rate of response observed for Au/W films under these conditions a reduction in sensitivity is also observed. This suggests that despite potentially enhancing the rate of dissociation of H$_2$, gold NPs may obstruct the available active sites on the tungsten oxide surface for reaction with H, which in addition to the apparent weak electronic interaction of gold NPs with tungsten oxide, as determined by the activation energy of conduction, diminish sensor response.

In summary, sensing tests of these devices show a high activity of platinum NPs compared to gold NPs most likely as a consequence of their reduced size, which favors their dispersion on tungsten oxide NNs, and formation of oxidized states in the shell surrounding the NP. These results suggest that to fully realize the advantages of metal-NP-functionalized MOX for sensing applications some metal NP features such as size, concentration, distribution must be controlled in order to improve the catalytic activity of the NPs and tune the characteristics at the NP/MOX interface. Modulation of AACVD parameters (e.g., initial solution concentration, flow rates, and fluxes) could effectively be optimized to adjust the metal NP features and we are currently carrying out further work to investigate these factors.

4. Conclusions

Tungsten oxide nanostructures functionalized with gold or platinum NPs have been synthesized and integrated, using a single-step method via AACVD, onto MEMS-based gas-sensor platforms. This co-deposition method has been demonstrated to be an effective route to incorporate metal NPs or combinations of metal NPs into nanostructured materials, resulting in an attractive way to tune functionality in metal oxides. Results have shown variations in electronic and sensing properties of tungsten oxide according to the metal NPs introduced, which have been used to effectively discriminate analytes (EtOH, H$_2$, and CO) present in proton-exchange fuel cells. Improved sensing characteristics, in particular to H$_2$, were observed at 250 °C with Pt-functionalized tungsten oxide films, whereas non-functionalized tungsten oxide films showed responses to low concentrations of CO at low temperatures (100 ppm, 150 °C). Differences in sensing characteristics of these films are attributed to the different reactivity of metal NPs (Au and Pt), and to the degree of electronic interaction at the MOX/metal NP interface. The method presented in this work is a promising technique to develop functional nanostructured MOX with the advantage of fewer step processes, relatively low processing temperature and no requirement for substrate pre-treatment. It is an industrially relevant and potentially scalable method for the production of functional nanomaterials and provides for their direct integration into device structures, as demonstrated by fabrication of MEMS microsensor arrays.

5. Experimental Section

Film Deposition: Tungsten oxide nanostructures functionalized with gold or platinum NPs were co-deposited at 400 °C via AACVD of tungsten hexaphenoxide (W(OPh)$_6$) (75 mg)[36] dissolved in acetone (12 mL, Sigma–Aldrich, ≥99.6%) and either tetrachloroauric acid trihydrate (HAuCl$_4$·3H$_2$O) (Sigma–Aldrich, 99.9%) (3.6 mg) or hexachloroplatinic acid hydrate (H$_2$PtCl$_6$·xH$_2$O) (Sigma–Aldrich, 99.9%) (3.8 mg) dissolved in methanol (Sigma–Aldrich, ≥99.6%) (3 mL) following a method reported previously.[12] A piezoelectric ultrasonic atomizer (Picfo) operated at 40 kHz was used to generate an aerosol of a mixture of the tungsten precursor and metal NP precursor. The aerosol droplets were transported to
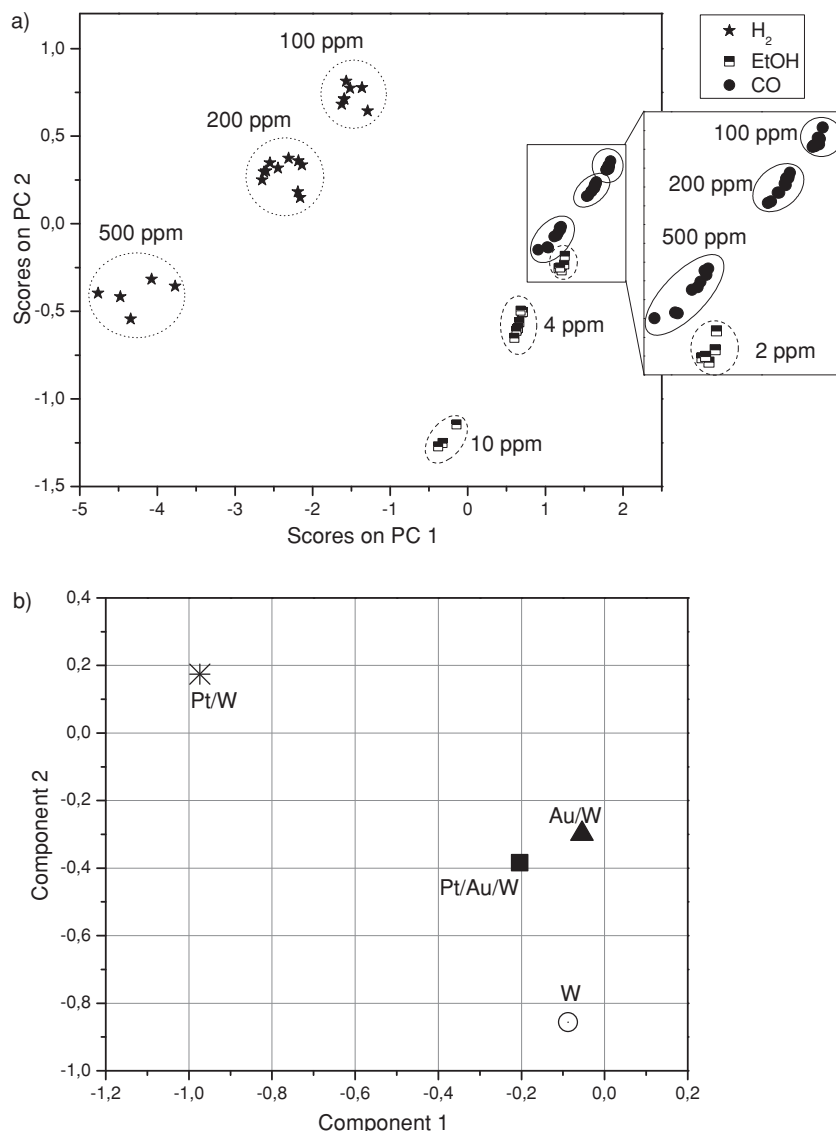
Materials
Views
www.MaterialsViews.com

ADVANCED
FUNCTIONAL
MATERIALS
www.afm-journal.de

FULL PAPER

Figure 10. Results of the PCA analysis of the sensor response, corresponding to the scores or projections of measurements in an orthogonal base of PCs (a) and loadings of each sensor to the principal components (b).

using monochromatic Al K_α radiation with 0.6 eV energy resolution; dual-beam charge neutralization from an electron gun ($\approx$1 eV) and argon-ion gun ($\leq$10 eV) for charge compensation. All of the binding energies were calibrated to the C 1s peak at 284.5 eV. To reproduce the Pt spectra, 2 doublets were used to fit the Pt 4f core level and the Shirley background. The procedure for fitting the spin-orbit doublet of Pt 4f has been reported previously.[28]

Sensor Technology: The microsensor substrates consist of a $SiO_2/Si_3N_4/SiO_2$ membrane (2 mm $\times$ 4.5 mm $\times$ 1.2 μm) with isolated platinum heaters and platinum electrodes (gap: 50 μm, thickness: 0.2 μm) deposited by sputtering in an area of 400 μm $\times$ 400 μm. The design and thermal characterization of the membrane has been described previously.[37] The sensing films were deposited on the microsensor substrate using a contact mask in order to protect the contacts and subsequently annealed and bonded in a TO-8 package.

Gas-Sensing Testing: Gas sensors were tested in a continuous flow (200 sccm) test chamber (280 cm^3 volume) that house 4 sensors, as previously described.[14a] The whole testing period comprised 6 months during which sensors were alternately tested to the analytes accumulating a total of $\approx$500 h of operation. During this period sensors were tested with operating temperatures between 100 and 300 °C, to various analytes and concentration performing up to ten replicates for each condition. Sensors were exposed to a given analyte and concentration for 10 min and subsequently the chamber purged with air until initial baseline resistance was recovered. To obtain the desired analyte concentration calibrated cylinders of either ethanol (Carburos Metálicos, 19.9 ppm ±1 ppm), hydrogen (Carburos Metálicos, 1000 ± 1 ppm) or carbon monoxide (Carburos Metálicos, 1000 ± 1 ppm) were mixed with pure synthetic air (Carburos Metálicos, 99.99%) by means of a mass flow system (Bronkhorst hi-tech 7.03.241). The sensor response was defined as $R = R_a/R_g$, where R_a is the sensor resistance in air and R_g represents the sensor resistance after 10 min of the analyte exposure.

the heated substrate by a nitrogen (oxygen-free) (BOC) gas flow (150 cm^3 min^{-1}). The time taken to transport the entire volume of solution was typically 60 minutes. Annealing of the samples was carried out in air at 500 °C for 2 h, heated from room temperature at 20 °C min^{-1} and subsequently allowed to cool to ambient. Silicon wafers (10 mm $\times$ 10 mm $\times$ 0.37 mm) were used as substrates for film analysis and cleaned with acetone and isopropyl alcohol prior to use, whereas MEMS-based substrates were used for gas-sensor fabrication (see sensor technology for details).

Film Analysis: The morphology of the samples was examined using scanning electron microscopy (SEM) (Jeol 6301F, 5 keV) and the structure using X-ray diffraction (XRD) (Bruker, AXD D8-Discover, using Cu K_α radiation operated at 40 kV and 40 mA). High-resolution TEM (HR-TEM) (Jeol 2100, 200 keV) was performed by removing the film from the substrate by sonication. The elemental and chemical composition were performed by means of wavelength dispersive X-ray (WDX) measurements (Philips, XL30ESEM) and X-ray photoelectron spectroscopy (XPS) (Physical Electronics, VERSAPROBE PHI 5000,

Supporting Information

Supporting Information is available from the Wiley Online Library or from the author.

FULL PAPER

[1] a) A. Gurlo, *Small* **2010**, *6*, 2077; b) M. E. Franke, T. J. Koplin, U. Simon, *Small* **2006**, *2*, 36.

[2] E. Comini, C. Baratto, G. Faglia, M. Ferroni, A. Vomiero, G. Sberveglieri, *Prog. Mater. Sci.* **2009**, *54*, 1.

[3] B. Roldan Cuenya, *Thin Solid Films* **2010**, *518*, 3127.

[4] E. Comini, *Anal. Chim. Acta* **2006**, *568*, 28.

[5] G. Korotcenkov, *Mater. Sci. Eng. R* **2008**, *61*, 1.

[6] B. R. Cuenya, *Thin Solid Films* **2010**, *518*, 3127.

[7] a) D. Koziej, M. Hubner, N. Barsan, U. Weimar, M. Sikora, J. D. Grunwaldt, *Phys. Chem. Chem. Phys.* **2009**, *11*, 8620; b) M. Hübner, D. Koziej, M. Bauer, N. Barsan, K. Kvashnina, M. D. Rossell, U. Weimar, J. D. Grunwaldt, *Angew. Chem. Int. Ed.* **2011**, *50*, 2841.

[8] R. G. Palgrave, I. P. Parkin, *J. Am. Chem. Soc.* **2006**, *128*, 1587.

[9] a) L. Armelao, D. Barreca, G. Bottaro, A. Gasparotto, S. Gross, C. Maragno, E. Tondello, *Coord. Chem. Rev.* **2006**, *250*, 1294; b) E. Della Gaspera, D. Buso, A. Martucci, *J. Sol-Gel Sci. Technol.* **2011**, *60*, 366; c) F. A. E. Flahaut, J. Sloan, C. O'Connor, M. L. H. Green, *Chem. Mater.* **2002**, *14*, 2553; d) B. Naoufal, K. Kohse-Höinghaus, T. Weimann, P. Hinze, S. Röhe, M. Bäumer, *Angew. Chem. Int. Ed.* **2011**, *50*, 9957.

[10] a) C. Klinke, J. B. Hannon, L. Gignac, K. Reuter, P. Avouris, *J. Phys. Chem. B* **2005**, *109*, 17787; b) Y. Liu, M. Liu, *Adv. Funct. Mater.* **2005**, *15*, 57.

[11] I. Simon, N. Bârsan, M. Bauer, U. Weimar, *Sens. Actuators, B* **2001**, *73*, 1.

[12] S. Vallejos, T. Stoycheva, P. Umek, C. Navio, R. Snyders, C. Bittencourt, E. Llobet, C. Blackman, S. Moniz, X. Correig, *Chem. Commun.* **2011**, *47*, 565.

[13] H. Zheng, J. Z. Ou, M. S. Strano, R. B. Kaner, A. Mitchell, K. Kalantar-zadeh, *Adv. Funct. Mater.* **2011**, *21*, 2175.

[14] a) S. Vallejos, V. Khatko, J. Calderer, I. Gracia, C. Canè, E. Llobet, X. Correig, *Sens. Actuators, B* **2008**, *132*, 209; b) T. Stoycheva, S. Vallejos, C. Blackman, S. J. A. Moniz, J. Calderer, X. Correig, *Sens. Actuators, B* **2012**, *161*, 406.

[15] a) A. Labidi, E. Gillet, R. Delamare, M. Maaref, K. Aguir, *Sens. Actuators, B* **2006**, *120*, 338; b) S. Vallejos, V. Khatko, K. Aguir, K. A. Ngo, J. Calderer, I. Gràcia, C. Cané, E. Llobet, X. Correig, *Sens. Actuators, B* **2007**, *126*, 573.

[16] J. Zhang, X. Liu, M. Xu, X. Guo, S. Wu, S. Zhang, S. Wang, *Sens. Actuators, B* **2010**, *147*, 185.

[17] a) L. F. Zhu, J. C. She, J. Y. Luo, S. Z. Deng, J. Chen, N. S. Xu, *J. Phys. Chem. C* **2010**, *114*, 15504; b) L. F. Zhu, J. C. She, J. Y. Luo, S. Z. Deng, J. Chen, X. W. Ji, N. S. Xu, *Sens. Actuators, B* **2011**, *153*, 354; c) Q. Xiang, G. F. Meng, H. B. Zhao, Y. Zhang, H. Li, W. J. Ma, J. Q. Xu, *J. Phys. Chem. C* **2010**, *114*, 2049.

[18] a) M. Stankova, X. Vilanova, J. Calderer, E. Llobet, J. Brezmes, I. Gràcia, C. Cané, X. Correig, *Sens. Actuators, B* **2006**, *113*, 241; b) D. J. Smith, J. F. Vatelino, R. S. Falconer, E. L. Wittman, *Sens. Actuators, B* **1993**, *13*, 264.

[19] A. Hierlemann, H. Baltes, *Analyst* **2003**, *128*, 15.

[20] a) J. L. Silveira, L. B. Braga, A. C. C. de Souza, J. S. Antunes, R. Zanzi, *Renewable Sustainable Energy Rev.* **2009**, *13*, 2525; b) N. Zamel, X. Li, *Prog. Energy Combust. Sci.* **2011**, *37*, 292.

[21] S. Vallejos, P. Umek, C. Blackman, *J. Nanosci. Nanotechnol.* **2011**, *11*, 8214.

[22] C. Navío, S. Vallejos, T. Stoycheva, E. Llobet, X. Correig, R. Snyders, C. Blackman, P. Umek, X. Ke, G. Van Tendeloo, C. Bittencourt, *Mater. Chem. Phys.* **2012**, *134*, 809.

[23] C. K. Tsung, W. B. Hong, Q. H. Shi, X. S. Kou, M. H. Yeung, J. F. Wang, G. D. Stucky, *Adv. Funct. Mater.* **2006**, *16*, 2225.

[24] J. M. Kim, H.-I. Joh, S. M. Jo, D. J. Ahn, H. Y. Ha, S.-A. Hong, S.-K. Kim, *Electrochim. Acta* **2010**, *55*, 4827.

[25] S. Ashraf, C. S. Blackman, S. C. Naisbitt, I. P. Parkin, *Meas. Sci. Technol.* **2008**, *19*, 1.

[26] S. Fischer, J. A. Martín-Gago, E. Román, K. D. Schierbaum, J. L. de Segovia, *J. Electron. Spectrosc. Relat. Phenom.* **1997**, *83*, 217.

[27] T. V. Choudrary, D. W. Goodman, *Top. Catal.* **2002**, *21*, 25.

[28] C. Bittencourt, M. Hecq, A. Felten, J. J. Pireaux, J. Ghijsen, M. P. Felicissimo, P. Rudolf, W. Drube, X. Ke, G. Van Tendeloo, *Chem. Phys. Lett.* **2008**, *462*, 260.

[29] R. Strobel, A. Alfons, S. E. Pratsinis, *Adv. Powder Technol.* **2006**, *17*, 457.

[30] H. S. Oh, J. H. Yang, C. K. Costello, Y. M. Wang, S. R. Bare, H. H. Kung, M. C. Kung, *J. Catal.* **2002**, *210*, 375.

[31] C. Zhang, A. Boudiba, C. Navio, C. Bittencourt, M.-G. Olivier, R. Snyders, M. Debliquy, *Int. J. Hydrogen Energy* **2011**, *36*, 1107.

[32] N. Barsan, U. Weimar, *J. Electroceram.* **2001**, *7*, 143.

[33] N. Yamazoe, K. Shimanoe, *Sens. Actuators, B* **2008**, *128*, 566.

[34] H. Abdi, L. J. Williams, *Wiley Interdiscip. Rev.: Comput. Stat.* **2010**, *2*, 433.

[35] L. Mädler, T. Sahm, A. Gurlo, J. D. Grunwaldt, N. Barsan, U. Weimar, S. E. Pratsinis, *J. Nanopart. Res.* **2006**, *8*, 783.

[36] W. B. Cross, I. P. Parkin, S. A. O'Neill, P. A. Williams, M. F. Mahon, K. C. Molloy, *Chem. Mater.* **2003**, *15*, 2786.

[37] R. Inglés, J. Pallares, I. Gràcia, A. M. Gué, J. L. Ramirez, *Sens. Actuators, B* **2011**, *172*, 124.